# **Generative Adversarial Method Based on Neural Tangent Kernels**

Yu-Rong Zhang\*

Sheng Yen Chou\*

Shan-Hung Wu\*

### **Abstract**

The recent development of Generative adversarial networks (GANs) has driven many computer vision applications. Despite the great synthesis quality, training GANs often confronts several issues, including non-convergence, mode collapse, and gradient vanishing. There exist several workarounds, for example, regularizing Lipschitz continuity and adopting Wasserstein distance. Although these methods can partially solve the problems, we argue that the problems are result from modeling the discriminator with deep neural networks. In this paper, we base on newly derived deep neural network theories called Neural Tangent Kernel (NTK) and propose a new generative algorithm called generative adversarial NTK (GA-NTK). The GA-NTK models the discriminator as a Gaussian Process (GP). With the help of the NTK theories, the training dynamics of GA-NTK can be described with a closed-form formula. To synthesize data with the closed-form formula, the objectives can be simplified into a single-level adversarial optimization problem. We conduct extensive experiments on real-world datasets, and the results show that GA-NTK can generate images comparable to those by GANs but is much easier to train under various conditions. We also study the current limitations of GA-NTK and propose some workarounds to make GA-NTK more practical.

## 1. Introduction

Generative adversarial networks (GANs) [16, 42], a branch of deep generative models based on adversarial learning, have received much attention due to their novel problem formulation and impressive performance in image synthesis. Variants of GANs has also driven recent developments of many computer vision tasks, such as superresolution [26], image inpainting [52], and video generation [50].

A GANs framework consists of a discriminator network  $\mathcal{D}$  and a generator network  $\mathcal{G}$  parametrized by  $\theta_{\mathcal{D}}$  and  $\theta_{\mathcal{G}}$ , respectively. Given an d-dimensional data distribution  $\mathcal{P}_{\text{data}}$ 

and a c-dimensional noise distribution  $\mathcal{P}_{\text{noise}}$ , the generator  $\mathcal{G}$  maps a random noise  $\mathbf{z} \in \mathbb{R}^c$  to a point  $\mathcal{G}(\mathbf{z}) \in \mathbb{R}^d$  in the data space, while the discriminator  $\mathcal{D}$  takes a point  $\mathbf{x}' \in \mathbb{R}^d$  as the input and tells whether  $\mathbf{x}'$  is real or fake, i.e.,  $\mathcal{D}(\mathbf{x}') = 1$  if  $\mathbf{x}' \sim \mathcal{P}_{\text{data}}$  and  $\mathcal{D}(\mathbf{x}') = 0$  if  $\mathbf{x}' \sim \mathcal{P}_{\text{gen}}$ , where  $\mathcal{P}_{\text{gen}}$  is the distribution of  $\mathcal{G}(\mathbf{z})$  and  $\mathbf{z} \sim \mathcal{P}_{\text{noise}}$ . The objective of GANs is typically formulated as a bilevel optimization problem:

$$\arg\min_{\boldsymbol{\theta}_{\mathcal{G}}} \max_{\boldsymbol{\theta}_{\mathcal{D}}} \mathbb{E}_{\boldsymbol{x} \sim \mathcal{P}_{\text{data}}} [\log \mathcal{D}(\boldsymbol{x})] + \mathbb{E}_{\boldsymbol{z} \sim \mathcal{P}_{\text{noise}}} [\log (1 - \mathcal{D}(\mathcal{G}(\boldsymbol{z})))]. \tag{1}$$

The discriminator  $\mathcal{D}$  and generator  $\mathcal{G}$  aim to break each other through the inner max and outer min objectives, respectively. The studies [16, 42] show that this adversarial formulation can lead to a better generator that produces plausible points/images.

However, GANs are known to be hard to train due to the following issues. Failure to Converge. In practice, Eq. (1) is usually only approximately solved by an alternating first-order method such as the alternating stochastic gradient descent (SGD). The alternating updates for  $\theta_D$  and  $\theta_C$ may cancel each other's progress. During each alternating training step, it is also tricky to balance the number of SGD updates for  $\theta_{\mathcal{D}}$  and that for  $\theta_{\mathcal{G}}$ , as a too small or large number for  $\theta_{\mathcal{D}}$  leads to low-quality gradients for  $\theta_{\mathcal{G}}$ . Mode **Collapse.** The alternating SGD is not good at distinguishing between a  $\min_{\theta_{\mathcal{G}}} \max_{\theta_{\mathcal{D}}} \text{ problem and a } \max_{\theta_{\mathcal{D}}} \min_{\theta_{\mathcal{G}}}$ problem. When the solution to the latter is returned, the generator tends to always produce the points at modes that best deceive the discriminator. The generated data will have low diversity. Vanishing Gradients. At the beginning of a training process, the finite real and fake training data may not overlap with each other in the data space, and thus the discriminator may be able to perfectly separate the real from fake data. Given the cross-entropy loss (or more generally, any f-divergence measure between  $\mathcal{P}_{\text{data}}$  and  $\mathcal{P}_{\text{gen}}$ ), the value of the discriminator becomes saturated on both sides of the decision boundary, resulting in zero gradients for  $\theta_G$ .

In this paper, we argue that the above issues are rooted in the modeling of  $\mathcal{D}$ . In most existing variants of GANs, the discriminator is a deep neural network with explicit weights  $\theta_{\mathcal{D}}$ . Under gradient descent, the gradients of  $\theta_{\mathcal{G}}$  in Eq. (1) cannot be back-propagated through the inner  $\max_{\theta_{\mathcal{D}}}$  problem because otherwise it requires the computation of high-

<sup>\*</sup>Department of Computer Science, National Tsing Hua University, Taiwan, R.O.C.. Correspondence to: Shan-Hung Wu<shwu@cs.nthu.edu.tw>.

order derivatives of  $\theta_{\mathcal{D}}$ . This motivates the use of alternating SGD, which in turn causes the convergence issues and mode collapse. Furthermore, the  $\mathcal{D}$  is a single network whose particularity may cause a catastrophic effect, such as the vanishing gradients, during training.

We instead model the discriminator  $\mathcal{D}$  as a Gaussian process (GP) whose mean and covariance are governed by a kernel function called the neural tangent kernel (NTK) [8,22,27]. The  $\mathcal{D}$  approximates an infinite ensemble of infinitely wide neural networks in a nonparametric manner and has no explicit weights. In particular, its training dynamics can be completely described by a closed-form formula. This allows us to simplify Eq. (1) into a single-level optimization problem, which we call the generative adversarial NTK (GA-NTK). Moreover, since  $\mathcal{D}$  is an infinite ensemble of networks, the particularity of a single element network does not drastically change the training process. GA-NTK gives no vanishing gradients and converges even with an f-divergence measure for each element network in  $\mathcal{D}$ . The following summarizes our contributions:

- We propose GA-NTK that, to the best of our knowledge, is the first single-level optimization method for adversarial data synthesis.
- GA-NTK can be solved by ordinary gradient descent, avoiding the convergence and mode collapse issues of alternating SGD during GANs training.
- GA-NTK does not incur vanishing gradients and works with any loss for D, including the cross-entropy loss that is cheap to evaluate and gives no side effects.
- We conduct extensive experiments on real-world datasets to study the advantages and limitations of GA-NTK. We find that GA-NTK is much easier to train than GANs, yet it consumes a significant amount of memory during training.
- We propose the batch-wise GA-NTK to improve the memory efficiency of the original GA-NTK and study the difference between these two variants.

Our work has implications for future research. In particular, GA-NTK bridges the gap between kernel methods and data/image synthesis and thus enables future studies on the relationship between kernels and generated images.

# 2. Related Work

Here, we briefly review GANs and their training techniques. We also give a background of NTKs.

#### 2.1. GANs and Improvements

The study [16] proposes GANs and gives a theoretical convergence guarantee in the function space. However, in

practice, one can only optimize the generator and discriminator in the parameter/weight space. This lead to many practical issues when solving Eq. (1).

Failure to Convergence. Given a large amount of weights in  $\theta_{\mathcal{G}}$  and  $\theta_{\mathcal{D}}$ , the alternating gradient descent algorithms are by far the most feasible methods to optimize the parameters of GANs. However, the alternating updates for  $\theta_{\mathcal{D}}$  and  $\theta_{\mathcal{G}}$  may cancel each other's progress. Also, these algorithms are sensitive to hyperparameters, such as the learning rate and the numbers of alternative training steps for  $\theta_{\mathcal{D}}$ and  $\theta_{\mathcal{G}}$ , respectively [31]. In particular, it is tricky to balance the numbers of training steps for  $heta_{\mathcal{D}}$  and  $heta_{\mathcal{G}}$  during each alternating training step. When the number for  $heta_{\mathcal{D}}$ is too small, the gradients of  $\theta_G$  will be meaningless because the discriminator is not trained. On the other hand, when the number is too large, the gradients of  $\theta_G$  will be unrepresentative since  $\mathcal{D}$  overfits the fake data in the current step. New training algorithms have been proposed for GANs [9, 37] or more general minimax problems [36, 49]. But recent works [12,33] show that there may not be a Nash equilibrium solution in GANs.

Mode Collapse. The alternating gradient descent algorithms are not good at distinguishing between a  $\min_{\theta_{\mathcal{G}}} \max_{\theta_{\mathcal{D}}} \text{ problem and a } \max_{\theta_{\mathcal{D}}} \min_{\theta_{\mathcal{G}}} \text{ problem be-}$ cause at optimality the gradients of  $heta_{\mathcal{D}}$  and  $heta_{\mathcal{G}}$  are zeros in both cases. Without second-order derivatives, the algorithms may return a solution to the latter problem. In this case, the generator tends to always produce the points at modes that best deceive the discriminator, decreasing the diversity of generated points. The study [34] alleviates this problem by back-propagating the computation of  $\theta_{\mathcal{G}}$  through the discriminators trained with several steps to strengthen the  $\min_{\theta_G} \max_{\theta_D}$  property. Other works mitigate mode collapse by diversifying the modes of  $\mathcal{D}$  through regularization [6,45,48] or modeling  $\mathcal{D}$  as an ensemble of multiple neural networks [11, 15].

Vanishing Gradients. At the beginning of a training process, the generated data may be very different from the real ones, causing disjoint  $\mathcal{P}_{data}$  and  $\mathcal{P}_{gen}$ . With a few inner  $\max_{\theta_{\mathcal{D}}}$  iterations, the discriminator may be able to perfectly separate the real from fake data. Given the crossentropy loss, the value of the discriminator becomes saturated on both sides of the decision boundary, which gives zero gradients for  $\theta_{\mathcal{G}}$ . The study [32] tries to solve this problem by using the Pearson  $\chi^2$ -divergence between  $\mathcal{P}_{\text{data}}$ and  $\mathcal{P}_{\text{gen}}$  as the loss to penalize data points that are far away from the decision boundary. However, it still suffers from vanishing gradients as any f-divergence measure, including the cross-entropy loss and Pearson  $\chi^2$ -divergence, cannot measure the difference between disjoint distributions [44]. Later studies replace the loss with either the Wasserstein distance [2, 18] or maximum mean discrepancy [17, 28, 29] that can measure the divergence of disjoint  $\mathcal{P}_{data}$  and  $\mathcal{P}_{gen}$ .

In addition, the works [35, 41] aim to constraint the Lipschitz continuity of the discriminator to prevent its value from being saturated.

Despite that many efforts have been made to improve the training of GANs, most existing approaches address only one or partial issues at a time with different assumptions, and in the meanwhile, they introduce new hyperparameters or side effects. For example, in the Wasserstein GANs [2, 18] mentioned above, efficient computation of Wasserstein distance requires the discriminator to be Lipschitz continuous. However, realizing Lipschitz continuity introduces new hyperparameters and limits the expressiveness of the discriminator. Until now, training GANs is still not an easy task because one has to tune many hyperparameters and to strike a balance between the benefits and costs of different training techniques to generate satisfactory points/images.

### 2.2. Neural Tangent Kernels

Consider an infinite ensemble of infinitely wide networks that use the mean square error (MSE) as loss and are trained by gradient descent. Recent developments in deep learning theory show that the prediction of the ensemble can be approximated by a special instance of Gaussian process (GP) called NTK-GP [8,22,27]. The NTK-GP is a Bayesian method, meaning that it outputs a distribution of possible values given an input point. The mean and covariance of the NTK-GP prediction are governed by a kernel function  $k(\cdot,\cdot)$  called the neural tangent kernel (NTK). Given two data points  $\boldsymbol{x}^i$  and  $\boldsymbol{x}^j$ , the  $k(\boldsymbol{x}^i, \boldsymbol{x}^j)$  represents the similarity score of the two points in a kernel space, which is fixed once the hyperparameters of the initial weights, activation function, and architecture of the networks in the target ensemble are determined.

Here, we focus on the mean prediction of NTK-GP as it is relevant to our study. Consider a supervised learning task given  $\mathbb{D}=(\boldsymbol{X}^n\in\mathbb{R}^{n\times d},\boldsymbol{Y}^n\in\mathbb{R}^{n\times c})$  as the training set, where there are n examples and each example consists of a pair of d-dimensional input and c-dimensional output. Let  $\boldsymbol{K}^{n,n}\in\mathbb{R}^{n\times n}$  be the kernel matrix for  $\boldsymbol{X}^n$ , i.e.,  $K_{i,j}^{n,n}=k(\boldsymbol{X}_{i,:}^n,\boldsymbol{X}_{j,:}^n)$ . Then, at time step t during gradient descent, the mean prediction of NTK-GP for  $\boldsymbol{X}^n$  evolve as

$$(\boldsymbol{I}^n - e^{-\eta \boldsymbol{K}^{n,n} t}) \boldsymbol{Y}^n \in \mathbb{R}^{n \times c},$$
 (2)

where  $I^n \in \mathbb{R}^{n \times n}$  is an identity matrix and  $\eta$  is a sufficiently small learning rate [22, 27].

The NTK used in Eq. (2) can be extended to support different network architectures, including convolutional neural networks (CNNs) [3, 14, 39, 53], recurrent neural networks (RNNs) [1, 54], networks with the attention mechanism [21], and other architectures [3, 54].

Note that a recent study [13] tries to explain the behavior of GANs from the NTK perspective. However, its discrim-

inator distinguishes between real data and pure noises (not generated data), which misses the adversarial nature. Our goals and modeling are very different from that work.

#### 3. GA-NTK

We present a new adversarial data synthesis method, called the generative adversarial NTK (GA-NTK), based on the NTK theory [8, 22, 27]. Given an unlabeled, ddimensional dataset  $X^n \in \mathbb{R}^{n \times d}$  of n points, we first augment  $\boldsymbol{X}^n$  to obtain a labeled training set  $\mathbb{D} = (\boldsymbol{X}^n \oplus \boldsymbol{Z}^n \in$  $\mathbb{R}^{2n\times d}, \mathbf{1}^n \oplus \mathbf{0}^n \in \mathbb{R}^{2n}$ ), where  $\mathbf{Z}^n \in \mathbb{R}^{n\times d}$  contains ngenerated points,  $\mathbf{1}^n \in \mathbb{R}^n$  and  $\mathbf{0}^n \in \mathbb{R}^n$  are label vectors of ones and zeros, respectively, and  $\oplus$  is the vertical stack operator. Then, we model a discriminator trained on  $\mathbb D$  as an NTK-GP. Let  $K^{2n,2n} \in \mathbb R^{2n \times 2n}$  be the kernel matrix for  $\boldsymbol{X}^n\oplus \boldsymbol{Z}^n$ , where the value each element  $K^{2n,2n}_{i,j}=k((\boldsymbol{X}^n\oplus \boldsymbol{Z}^n)_{i,:},(\boldsymbol{X}^n\oplus \boldsymbol{Z}^n)_{j,:})$  can be computed once we decide the initialization, activation function, and architecture of the element networks in the target infinite ensemble, i.e., the discriminator. By Eq. (2) and let  $\lambda = \eta \cdot t$ , the mean prediction of the discriminator can be written as

$$\mathcal{D}(\boldsymbol{X}^n, \boldsymbol{Z}^n; k, \lambda) = (\boldsymbol{I}^{2n} - e^{-\lambda \boldsymbol{K}^{2n,2n}})(\boldsymbol{1}^n \oplus \boldsymbol{0}^n) \in \mathbb{R}^{2n},$$
(3)

where  $I^{2n} \in \mathbb{R}^{2n \times 2n}$  is an identity matrix. We formulate the objective of GA-NTK as follows:

$$\arg\min_{\boldsymbol{Z}^n} \|\mathbf{1}^{2n} - \mathcal{D}(\boldsymbol{X}^n, \boldsymbol{Z}^n; k, \lambda)\|_2, \tag{4}$$

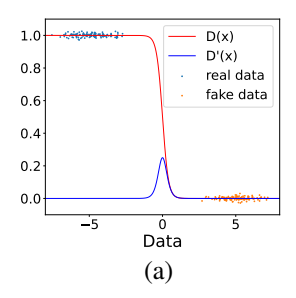
where  $\mathbf{1}^{2n} \in \mathbb{R}^{2n}$  is a vector of ones. GA-NTK aims to find points  $\mathbf{Z}^n$  that best deceives the discriminator such that it outputs wrong labels  $\mathbf{1}^{2n}$  for these points. On the other hand, the discriminator is trained on  $\mathbb D$  with the correct labels  $\mathbf{1}^n \oplus \mathbf{0}^n$  and therefore has the opposite goal of distinguishing between the real and generated points.

GA-NTK formulates an adversarial data synthesis task as a single-level optimization problem. This is achievable because the dynamics of the prediction made by the discriminator during gradient descent can be completely described by a closed-form formula in Eq. (3). Therefore, one can easily solve Eq. (4) by 1) randomly initiating  $\mathbf{Z}^n$ , and 2) updating  $\mathbf{Z}^n$  using the ordinary gradient descent steps. With different initial values, the resulting points in  $\mathbf{Z}^n$  may be different, giving creativity.

#### 3.1. Merits

As compared to GANs, GA-NTK offers the following advantages in training:

**Convergence.** The GA-NTK can be trained by ordinary gradient descent. This gives much nicer convergence properties because there is no alternating updates that may



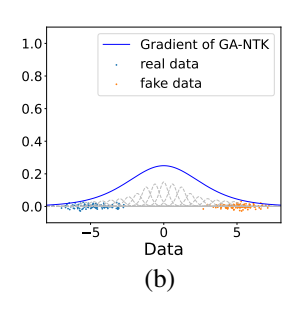


Figure 1. Decision boundary of the discriminator and the corresponding gradients for the generator/ $\mathbb{Z}^n$  in (a) GANs and (b) GANTK at the beginning of the training process over a 1D toy dataset. The gray dashed lines indicate the gradients for  $\mathbb{Z}^n$  from different element networks of the ensemble discriminator in GA-NTK.

cancel each other's progress, and there is no confusion between the min-max and max-min problems during gradient descent as in the alternating SGD used for training GANs.

No Vanishing Gradients, No Side Effects. As shown in Figure 1, the discriminator  $\mathcal{D}$  is an infinite ensemble of networks whose value never saturates. Therefore, it can always provide the gradients for  $\mathbb{Z}^n$  in Eq. (4). There is no need for an expensive loss for  $\mathcal{D}$ , such as the Wasserstein distance [2, 18] whose efficient evaluation requires Lipschitz continuity (and hence limited expressiveness) of  $\mathcal{D}$ .

**Hyperparameter Tuning.** The computation of  $K^{2n,2n}$ requires one to determine the initialization and architecture of the element networks in the ensemble discriminator. Studies [40, 43, 46] have proposed a principled method to tune the hyperparameters for the initialization. From our empirical results, we also find that the quality of the images generated by GA-NTK is not significantly impacted by the choice of the architecture—a fully connected network with rectified linear unit (ReLU) activation suffices to generate recognizable image patterns. Once  $K^{2n,2n}$  is decided, there is only one hyperparameter  $\lambda$  to tune in Eq. (4). The  $\lambda$  controls how well the discriminator is trained on  $\mathbb{D}$ , so either a too small or large value can lead to poor gradients for  $Z^n$ and final generated points. But since there is no alternating updates as in GANs, we can decide an appropriate value of  $\lambda$  without worrying about canceling the learning progress of  $\mathbb{Z}^n$ . We propose a simple algorithm for tuning  $\lambda$ , as shown in Algorithm 1. Basically, we search for a value that makes the discriminator nearly separate the real data from pure noises in an auxiliary learning task, and then use this value to solve Eq. (4). In practice, a small positive  $\epsilon$  ranging from  $10^{-3}$  to  $10^{-2}$  suffices to give an appropriate  $\lambda$ .

**Algorithm 1** Searching  $\lambda$  for GA-NTK.

**Input:** Data  $X^n$ , kernel k, and separation tolerance  $\epsilon$ 

**Output:**  $\lambda$  for GA-NTK

Randomly initiate  $\boldsymbol{Z}^n \in \mathbb{R}^{n \times d}$ 

 $\lambda \leftarrow 1$ 

while  $\frac{1}{2n}\|\mathcal{D}(\boldsymbol{X}^n,\boldsymbol{Z}^n;k,\lambda)-(\mathbf{1}^n\oplus\mathbf{0}^n)\|_2^2\leq\epsilon$  do

end

return  $\lambda$ 

#### 3.2. GA-NTK in Practice

To generate more points than the real data in  $X^n$ , we can parallelly solve multiple  $Z^n$ 's in Eq. (4) on different machines. With different initial values, these  $Z^n$ 's can contain different synthesized points.

On a single machine, the gradients of  $Z^n$  needs to be back-propagated through the computation of  $K^{2n,2n}$ , which has  $O(n^2)$  space complexity. This may incur scalability issues for large datasets. Although recent efforts [3,5,19] have been made to reduce the time and space complexity of the evaluation of NTK and its variants, they are still at an early stage of development and the consumed space in practice may still be too large. To alleviate this problem, we propose the batch-wise GA-NTK that solves Eq. (4) using mini-batches: during each gradient descent iteration, we 1) randomly sample a batch of rows in  $X^n \oplus Z^n$ and their corresponding labels, and 2) calculate the gradients of  $\mathbb{Z}^n$  only based on  $\mathbb{K}^{b,b}$ , where b is the batch size. Although the batch-wise GA-NTK is cosmetically similar to the original GA-NTK, it solves a different problem. In the original GA-NTK, the  $Z^n$  aims to fool a single discriminator  $\mathcal{D}$  trained on 2n examples, while in the batch-wise GA-NTK, the  $\mathbb{Z}^n$ 's goal is to deceive many discriminators, each trained on b examples only. Fortunately, studies [4,47] have shown that NTK-based methods perform well on small datasets. So, with a large enough b, the batch-wise GA-NTK may be a practical solution. We will investigate the difference between the original GA-NTK and batch-wise GA-NTK in more detail in Section 4.

## 4. Experiments

In this section, we conduct experiments to study how GA-NTK works and its limitations.

**Datasets.** We consider the unsupervised/unconditional image synthesis tasks over real-world datasets, including MNIST [25], CIFAR-10 [24], CelebA [30], and ImageNet [10]. To improve training efficiency, we resize CelebA images to 64×64 and ImageNet images to 128×128 pixels, respectively. We also create a 2D toy dataset consisting of 25-modal Gaussian mixtures of points to visualize the behavior of different image synthesis methods.

 $<sup>^1</sup>$ This does not imply that the discriminator  $\mathcal D$  has low model complexity. In Eq. (3), the predictions of the  $\mathcal D$  for the 2n input points  $\boldsymbol X^n\oplus \boldsymbol Z^n$  converge to the correct babels  $\boldsymbol 1^n\oplus \boldsymbol 0^n$  as  $t\to\infty$ . The discriminator always has enough model complexity to (over-)fit the training data.



Figure 2. The images generated by different methods on MNIST, CIFAR-10, and CelebA datasets given only 256 training images.

GA-NTK implementations. GA-NTK works with different NTKs. For the image synthesis tasks, we consider the NTKs that models the ensembles of fully-connected networks [8, 22, 27] and convolutional networks [3, 14, 39, 53], respectively. We implement GA-NTK using the Neural Tangents library [38] and call our implementations using the former and latter NTKs the GA-FNTK and GA-CNTK, respectively. In GA-FNTK, an element network of the discriminator has 3 infinitely wide, fully-connected layers with ReLU non-linearity, while in GA-CNTK, an element network follows the architecture of InfoGAN [7] except having infinite filters at each layer. We tune the hyperparameters of GA-FNTK and GA-CNTK following the steps described in Section 3.1 and Algorithm 1.

**Baselines.** We compare GA-NTK with some popular variants of GANs, including vanilla GANs [16], DC-GAN [42], LSGAN [32], WGAN [2], WGAN-GP [18], and SNGAN [35]. To give a fair comparison, we let the dis-

criminator of each baseline follow the architecture of Info-GAN [7] and tune the hyperparameters using grid search.

**Metrics.** We evaluate the quality of a set of generated images using the Frechet Inception Distance (FID) [20]. We find that an image synthesis method may produce downgrade images that look almost identical to some images in the training set. Therefore, we also use a metric called the average max-SSIM (AM-SSIM) that calculates the average of the maximum SSIM score [51] between  $\mathcal{P}_{\text{gen}}$  and  $\mathcal{P}_{\text{data}}$ :

$$\text{AM-SSIM}(\mathcal{P}_{\text{gen}}, \mathcal{P}_{\text{data}}) = \mathbb{E}_{\boldsymbol{x}' \sim \mathcal{P}_{\text{gen}}}[\max_{\boldsymbol{x} \sim \mathcal{P}_{\text{data}}} \text{SSIM}(\boldsymbol{x}', \boldsymbol{x})].$$

A generated image set will have a higher AM-SSIM score if it contains downgrade images.

Environment and Limitations. We conduct all experiments on a cluster of machines having 80 NVIDIA Tesla V100 GPUs. As discussed in 3.2, GA-NTK consumes a significant amount of memory on each machine due to the computations involved in the kernel matrix  $K^{2n,2n}$ . With

Table 1.	The FID	and AM-	SSIM scor	res of the	images	generated by	y different methods.

	Data size	Metric	DCGAN	LSGAN	WGAN	WGAN-GP	SN-GAN	GA-NTK
MNIST	64	FID	27.43	69.76	50.69	32.49	57.89	31.10
	0.1	AM-SSIM	0.84	0.79	0.77	0.83	0.67	0.49
	128	FID	31.89	38.52	49.28	30.20	38.33	21.14
		AM-SSIM	0.85	0.80	0.74	0.76	0.67	0.52
	256	FID	69.76	35.33	50.33	24.37	29.49	14.96
	200	AM-SSIM	0.69	0.78	0.72	0.73	0.70	0.54
CIFAR-10	64	FID	312.21	258.41	117.85	49.29	118.16	55.54
	0.	AM-SSIM	0.22	0.25	0.29	0.74	0.28	0.41
	128	FID	229.94	339.27	101.90	68.53	128.65	39.98
	120	AM-SSIM	0.36	0.10	0.26	0.60	0.21	0.41
	256	FID	181.15	255.19	111.92	85.34	107.29	28.40
	230	AM-SSIM	0.27	0.22	0.22	0.46	0.20	0.42
CelebA	64	FID	489.82	83.71	122.36	83.71	169.04	30.83
		AM-SSIM	0.02	0.05	0.29	0.56	0.29	0.60
	128	FID	55.01	450.81	125.82	92.73	168.11	33.51
		AM-SSIM	0.03	0.11	0.28	0.54	0.28	0.51
	256	FID	461.95	403.79	108.07	79.36	161.20	63.15
		AM-SSIM	0.04	0.09	0.31	0.39	0.27	0.38

the current version of Neural Tangents library [38] and a V100 GPU of 32GB RAM, the maximum sizes of the training set from MNIST, CIFAR-10, CelebA, and ImageNet are 1024, 512, 256, and 128, respectively (where the computation graph and backprop operations of  $K^{2n,2n}$  consume about 27.5 GB RAM excluding other necessary operations). Since our goal is not to achieve the state-of-the-art performance but to compare between different image synthesis methods, we train all the methods using up to 256 images randomly sampled from all classes of MNIST, the "horse" class CIFAR-10, the "male with straight hair" class of CelebA, and the "daisy" class of ImageNet, respectively. We will conduct larger-scale experiments in Section 4.2. For more details about our experiment settings, please see the supplementary file.

### 4.1. **GA-NTK**

We first study the quality of the images synthesized by different methods. Table 1 summarizes the FID and AM-SSIM scores of the generated images, and Figure 2 shows some samples of them. As we can see, the baselines, including LSGAN and DCGAN, that use f-divergence as the loss function give worse images due to the various training

issues mentioned above. Other methods, including WGAN, WGAN-GP, and SN-GAN, can successfully generate images. In particular, WGAN-GP performs the best among the baselines. However, WGAN-GP limits the Lipschitz continuity of the discriminator and gives higher FID scores than GA-CNTK. Also, it gives higher AM-SSIM values as the size of the training set decreases, implying there are many downgrade images that look identical to some training images. This is because the Wasserstein distance, which is also called the earth mover's distance, allows fewer ways of moving given less "earth" (i.e., the density values of  $\mathcal{P}_{\text{data}}$  and  $\mathcal{P}_{\text{gen}}$ ), and thus the  $\mathcal{P}_{\text{gen}}$  needs to be exactly the same as  $\mathcal{P}_{\text{data}}$  to minimizes the distance.

In summary, GA-CNTK can achieve comparable (if not better) performance as the existing variants of GANs. Next, we study its training behavior.

Convergence. Figure 3 shows the learning curve and the relationship between the image quality and the number of gradient descent iterations during a training process of GA-CNTK. Since the objective of GA-CNTK is a single-level optimization problem, the gradient descent always converges. More importantly, we can see a correlation between the image quality and the loss value—as the

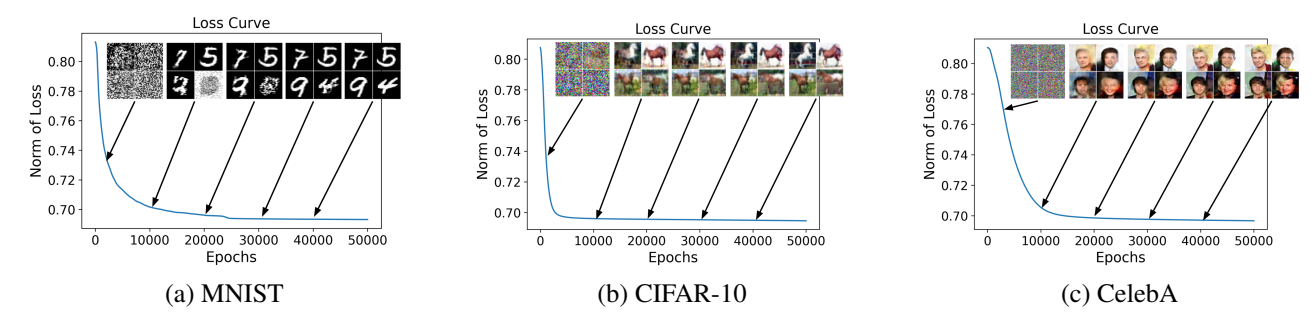


Figure 3. The learning curve and image quality at different stages of a training process.

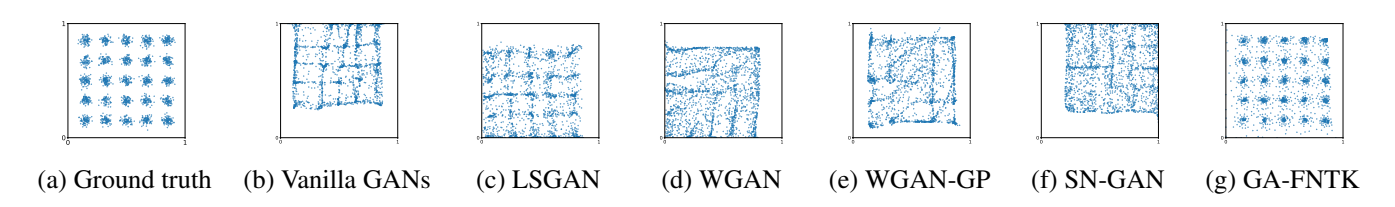


Figure 4. Visualization of distribution alignment and mode collapse on a 2D toy dataset.

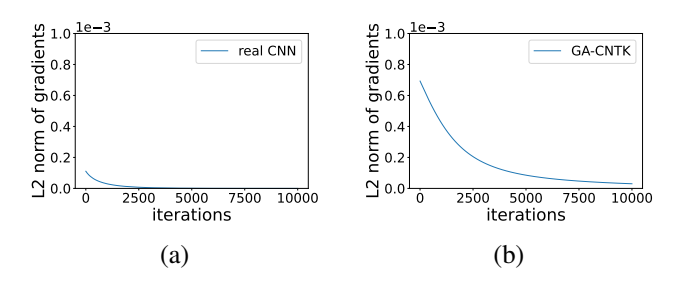


Figure 5. Comparison between the gradients of a  $Z_{i,:}$  in Eq. (4) obtained from the (a) finite- and (b) infinite-width discriminators.

loss becomes smaller, the quality of the synthesized images improves. This correlation can save human labor from monitoring the indefinite training processes of GANs.

**Mode Collapse.** To study how different methods align  $\mathcal{P}_{gen}$  with  $\mathcal{P}_{data}$ , we train them using a 2D toy training set where  $\mathcal{P}_{data}$  is a 25-modal Gaussian mixture. We use two 3-layer FNNs as the generator and discriminator for each baseline and an ensemble of 3-layer, infinitely wide FNN as the discriminator in GA-FNTK. For GANs, we stop the alternating SGD training when the generator receives 1000 updates, and for GA-FNTK, we terminate the GD training after 1000 iterations. Figure 4 shows the resultant  $\mathcal{P}_{gen}$  of different methods. By avoiding the use of alternating SGD, GA-FNTK is free from mode collapse.

**Gradient Vanishing.** To verify that GA-NTK gives no vanishing gradients as Figure 1 shows, we conduct an experiment using another toy dataset consisting of 256 MNIST images and 256 random noises. We replace the discriminator of GA-CNTK with a single parametric net-

work of the same architecture but finite width. We train the finite-width network on the toy dataset by minimizing the MSE loss using gradient descent. We set the training iteration to a large vale (65536) to simulate the situation where the network value becomes saturated on both sides of the decision boundary. Figure 5 compares between the gradients of a generated image  $Z_{i,:}^n$  in Eq. (4) obtained from the finite-width network and the corresponding GA-CNTK with a large t. As  $Z_{i,:}^n$  evolves through gradient descent iterations, the norm of its gradients obtained from the finite-width discriminator quickly shrinks to zero. On the other hand, the gradient norm obtained from the discriminator of GA-CNTK is always positive thanks to the infinite ensembling. GA-NTK does not suffer from gradient vanishing.

# 4.2. Batch-Wise GA-NTK

To work with a larger training set, we modify GA-CNTK by following the instructions in Section 3.2 to obtain the batch-wise GA-CNTK, which computes the gradients of  $\mathbb{Z}^n$  in Eq. (4) from 256 randomly sampled training images during each gradient descent iteration. We train the batch-wise GA-CNTK on two larger datasets consisting of 2048 images from CelebA and 1300 images from ImageNet, respectively. Figure 6(b) shows that the batch-wise GA-CNTK can successfully generate the "daisy" images on ImageNet.

Note that the batch-wise GA-CNTK solves a different problem than the original GA-CNTK—the former finds  $\mathbb{Z}^n$  that deceives *multiple* discriminators, each trained on 256 examples, while the latter searches for  $\mathbb{Z}^n$  that fools a single discriminator trained on 256 examples. Comparing the images in Figure 2(f) with those in Figure 6(a), we can see that

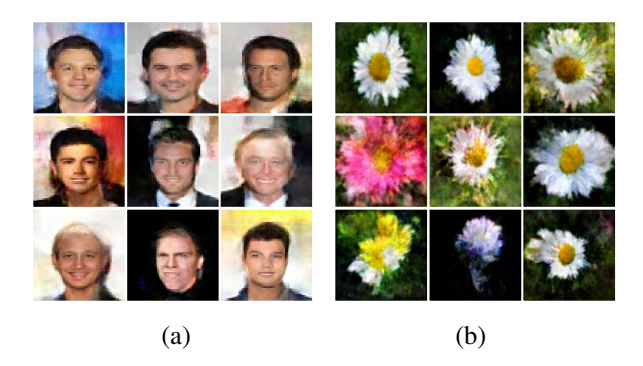


Figure 6. The images generated by batch-wise GA-CNTK on (a) sampled CelebA dataset of 2048 images and (b) sampled ImageNet dataset of 1300 images.

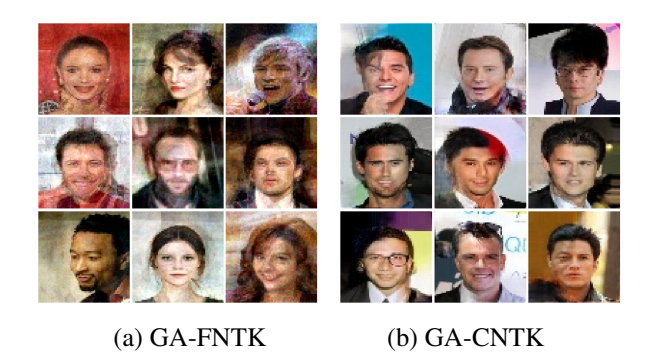


Figure 7. The images generated by (a) GA-FNTK and (b) GA-CNTK given 256 CelebA training images.

the batch-wise GA-CNTK gives a little more blurry images but the patterns in each synthesized image are more globally coherent, both due to the effect of multiple discriminators.

#### 4.3. Ablation Study

GA-FNTK vs. GA-CNTK. So far, we only show the images generated by GA-CNTK. Figure 7 compares between the images generated by GA-FNTK and GA-CNTK. To our surprise, modeling the discriminator as an ensemble of fully connected networks suffices to generate recognizable faces. Generally, we find that the images synthesized by GA-FNTK are less crispy but have better global coherence than those generated by GA-CNTK. This is because a CNTK performs convolutions and learns only the shift-invariant patterns. This motivates techniques for enhancing the global coherence in GA-CNTK, and our proposed batch-wise training technique could be a solution.

**Sensitivity to Hyperparameters.** Here, we study how sensitive is the performance of WGAN, WGAN-GP, and GA-FNTK to hyperparameters. We adjust the hyperparameters of different approaches using the grid search for WGAN and WGAN-GP and Algorithm 1 for GA-FNTK, respectively, under a time budget of 3 hours, and then eval-

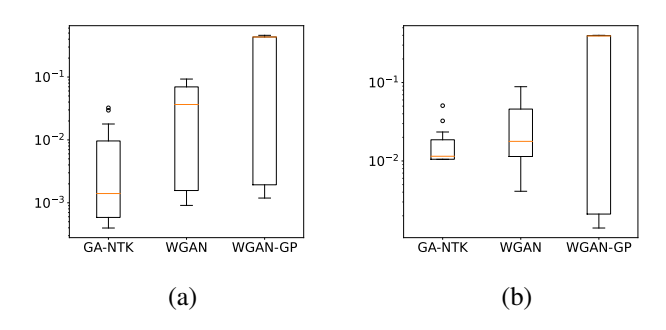


Figure 8. The distribution of Wasserstein distance between  $\mathcal{P}_{\text{gen}}$  and  $\mathcal{P}_{\text{data}}$  (used to measure the quality of the generated points) over the searched hyper-parameters on training sets of (a) 8- and (b) 25-modal Gaussian mixtures.

uate the quality of the generated images by the Wasserstein distance between  $\mathcal{P}_{gen}$  and  $\mathcal{P}_{data}$ . We train different methods on two toy datasets consisting of 8- and 25-modal Gaussian mixtures following the settings described in the Mode Collapse paragraph in Section 4.1. For WGAN, we search the weight clipping boundary from 0.01, and for WGAN-GP, we search the gradient penalty parameter from 10, which both follow the original papers [2, 18]. For GA-FNTK, we run Algorithm 1 to obtain an initial  $\lambda$ , and then, after reaching 1000 GD iterations, we use grid search to tune the final  $\lambda$ . We sample 2048 generated data to evaluate the Wasserstein distance.

Figure 8 shows the results. GA-FNTK achieves the lowest average Wasserstein distances, and the variances are smaller than the two other baselines, too. This shows that the performance of GA-FNTK is less sensitive the hyperparameter  $\lambda$  and is easier to tune in practice.

We have conducted more experiments, and the results can be found in the supplementary file.

## 5. Conclusion

Based on the recent developments of neural tenant kernels (NTKs), we proposed a new adversarial data synthesis approach called the generative adversarial NTK (GA-NTK) that models the discriminator as a Gaussian process (GP) whose training dynamics can be completely described by a closed-form formula. To the best of our knowledge, GA-NTK is the first single-level optimization method for adversarial data synthesis and can be solved by ordinary gradient descent. We conducted extensive experiments on real-world datasets, and the results demonstrate that GA-NTK can avoid the problems of convergence, mode collapse, and gradient vanishing in GANs simultaneously.

Our work has implications for future research. In particular, GA-NTK bridges the gap between kernel methods and data/image synthesis. This motivates future studies on the

relationship between kernels and generated images. We also identified some current limitations of GA-NTK, including the memory issue and the lack of global coherency in GA-CNTK synthesized images. Further improvements on these aspects are matters of our future inquiry.

#### References

- [1] Sina Alemohammad, Zichao Wang, Randall Balestriero, and Richard G. Baraniuk. The recurrent neural tangent kernel. In *Proc. of ICLR*, 2021.
- [2] Martin Arjovsky, Soumith Chintala, and Léon Bottou. Wasserstein generative adversarial networks. In *Proc. of ICML*, 2017. 2, 3, 4, 5, 8
- [3] Sanjeev Arora, Simon S. Du, Wei Hu, Zhiyuan Li, Ruslan Salakhutdinov, and Ruosong Wang. On exact computation with an infinitely wide neural net. In *Proc. of NeurIPS*, 2019. 3, 4, 5
- [4] Sanjeev Arora, Simon S. Du, Zhiyuan Li, Ruslan Salakhutdinov, Ruosong Wang, and Dingli Yu. Harnessing the power of infinitely wide deep nets on small-data tasks. In *Proc. of ICLR*, 2020. 4
- [5] Alberto Bietti and Julien Mairal. On the inductive bias of neural tangent kernels. In *Proc. of NeurIPS*, 2019.
- [6] Tong Che, Yanran Li, Athul Paul Jacob, Yoshua Bengio, and Wenjie Li. Mode regularized generative adversarial networks. In *Proc. of ICLR*, 2017. 2
- [7] Xi Chen, Yan Duan, Rein Houthooft, John Schulman, Ilya Sutskever, and Pieter Abbeel. Infogan: Interpretable representation learning by information maximizing generative adversarial nets. In *Proc. of NeurIPS*, 2016. 5, 12
- [8] Lenaic Chizat, Edouard Oyallon, and Francis Bach. On lazy training in differentiable programming. In *Proc. of NeurIPS*, 2019. 2, 3, 5
- [9] Constantinos Daskalakis, Andrew Ilyas, Vasilis Syrgkanis, and Haoyang Zeng. Training gans with optimism. In *Proc. of ICLR*, 2018.
- [10] Jia Deng, Wei Dong, Richard Socher, Li-Jia Li, Kai Li, and Li Fei-Fei. Imagenet: A large-scale hierarchical image database. In *Proc. of CVPR*, 2009. 4
- [11] Ishan P. Durugkar, Ian Gemp, and Sridhar Mahadevan. Generative multi-adversarial networks. In *Proc. of ICLR*, 2017. 2
- [12] Farzan Farnia and Asuman E. Ozdaglar. Do gans always have nash equilibria? In *Proc. of ICML*, 2020.
- [13] Jean-Yves Franceschi, Emmanuel de Bézenac, Ibrahim Ayed, Mickaël Chen, Sylvain Lamprier, and

- Patrick Gallinari. A neural tangent kernel perspective of gans. *CoRR*, abs/2106.05566, 2021. 3
- [14] Adrià Garriga-Alonso, Carl Edward Rasmussen, and Laurence Aitchison. Deep convolutional networks as shallow gaussian processes. In *Proc. of ICLR*, 2019. 3, 5
- [15] Arnab Ghosh, Viveka Kulharia, Vinay P. Namboodiri, Philip H. S. Torr, and Puneet Kumar Dokania. Multi-agent diverse generative adversarial networks. In *Proc. of CVPR*, 2018. 2
- [16] Ian Goodfellow, Jean Pouget-Abadie, Mehdi Mirza, Bing Xu, David Warde-Farley, Sherjil Ozair, Aaron Courville, and Yoshua Bengio. Generative adversarial nets. In *Proc. of NeurIPS*, 2014. 1, 2, 5
- [17] Arthur Gretton, Karsten M. Borgwardt, Malte J. Rasch, Bernhard Schölkopf, and Alexander J. Smola. A kernel two-sample test. *J. Mach. Learn. Res.*, 2012.
- [18] Ishaan Gulrajani, Faruk Ahmed, Martín Arjovsky, Vincent Dumoulin, and Aaron C. Courville. Improved training of wasserstein gans. In *Proc. of NeurIPS*, 2017. 2, 3, 4, 5, 8
- [19] Insu Han, Haim Avron, Neta Shoham, Chaewon Kim, and Jinwoo Shin. Random features for the neural tangent kernel. *CoRR*, abs/2104.01351, 2021. 4
- [20] Martin Heusel, Hubert Ramsauer, Thomas Unterthiner, Bernhard Nessler, and Sepp Hochreiter. Gans trained by a two time-scale update rule converge to a local nash equilibrium. In *Proc. of NeurIPS*, 2017.
  5, 13
- [21] Jiri Hron, Yasaman Bahri, Jascha Sohl-Dickstein, and Roman Novak. Infinite attention: NNGP and NTK for deep attention networks. In *Proc. of ICML*, 2020. 3
- [22] Arthur Jacot, Franck Gabriel, and Clement Hongler. Neural tangent kernel: Convergence and generalization in neural networks. In *Proc. of NeurIPS*, 2018. 2, 3, 5
- [23] Diederik P. Kingma and Jimmy Ba. Adam: A method for stochastic optimization. In *Proc. of ICLR*, 2015.
- [24] Alex Krizhevsky. Learning multiple layers of features from tiny images. Technical report, 2009. 4
- [25] Yann LeCun, Corinna Cortes, and CJ Burges. Mnist handwritten digit database. *ATT Labs [Online]. Available: http://yann.lecun.com/exdb/mnist*, 2, 2010. 4
- [26] Christian Ledig, Lucas Theis, Ferenc Huszar, Jose Caballero, Andrew Cunningham, Alejandro Acosta, Andrew P. Aitken, Alykhan Tejani, Johannes Totz, Zehan Wang, and Wenzhe Shi. Photo-realistic single image super-resolution using a generative adversarial network. In *Proc. of CVPR*, 2017. 1

- [27] Jaehoon Lee, Lechao Xiao, Samuel Schoenholz, Yasaman Bahri, Roman Novak, Jascha Sohl-Dickstein, and Jeffrey Pennington. Wide neural networks of any depth evolve as linear models under gradient descent. In *Proc. of NeurIPS*, 2019. 2, 3, 5
- [28] Chun-Liang Li, Wei-Cheng Chang, Yu Cheng, Yiming Yang, and Barnabás Póczos. MMD GAN: towards deeper understanding of moment matching network. In *Proc. of NeurIPS*, 2017.
- [29] Yujia Li, Kevin Swersky, and Richard S. Zemel. Generative moment matching networks. In *Proc. of ICML*, 2015. 2
- [30] Ziwei Liu, Ping Luo, Xiaogang Wang, and Xiaoou Tang. Deep learning face attributes in the wild. In *Proc. of ICCV*, December 2015. 4, 18
- [31] Mario Lucic, Karol Kurach, Marcin Michalski, Sylvain Gelly, and Olivier Bousquet. Are gans created equal? A large-scale study. In *Proc. of NeurIPS*, 2018. 2, 12
- [32] Xudong Mao, Qing Li, Haoran Xie, Raymond Y. K. Lau, Zhen Wang, and Stephen Paul Smolley. Least squares generative adversarial networks. In *Proc. of ICCV*, 2017. 2, 5, 13
- [33] Lars M. Mescheder, Andreas Geiger, and Sebastian Nowozin. Which training methods for gans do actually converge? In *Proc. of ICML*, 2018. 2
- [34] Luke Metz, Ben Poole, David Pfau, and Jascha Sohl-Dickstein. Unrolled generative adversarial networks. In *Proc. of ICLR*, 2017. 2
- [35] Takeru Miyato, Toshiki Kataoka, Masanori Koyama, and Yuichi Yoshida. Spectral normalization for generative adversarial networks. In *Proc. of ICLR*, 2018. 3, 5
- [36] Aryan Mokhtari, Asuman E. Ozdaglar, and Sarath Pattathil. A unified analysis of extra-gradient and optimistic gradient methods for saddle point problems: Proximal point approach. In *Proc. of AISTATS*, 2020.
- [37] Vaishnavh Nagarajan and J. Zico Kolter. Gradient descent GAN optimization is locally stable. In *Proc. of NeurIPS*, 2017. 2
- [38] Roman Novak, Lechao Xiao, Jiri Hron, Jaehoon Lee, Alexander A Alemi, Jascha Sohl-Dickstein, and Samuel S Schoenholz. Neural tangents: Fast and easy infinite neural networks in python. In *Proc. of ICLR*, 2019. 5, 6
- [39] Roman Novak, Lechao Xiao, Jaehoon Lee, Yasaman Bahri, Greg Yang, Jiri Hron, Daniel A. Abolafia, Jeffrey Pennington, and Jascha Sohl-Dickstein. Bayesian deep convolutional networks with many channels are gaussian processes. In *Proc. of ICLR*, 2019. 3, 5

- [40] Ben Poole, Subhaneil Lahiri, Maithra Raghu, Jascha Sohl-Dickstein, and Surya Ganguli. Exponential expressivity in deep neural networks through transient chaos. In *Proc. of NeurIPS*, 2016. 4
- [41] Guo-Jun Qi. Loss-sensitive generative adversarial networks on lipschitz densities. *Int. J. Comput. Vis.*, 2020.
- [42] Alec Radford, Luke Metz, and Soumith Chintala. Unsupervised representation learning with deep convolutional generative adversarial networks. In *Proc. of ICLR*, 2016. 1, 5
- [43] Maithra Raghu, Ben Poole, Jon M. Kleinberg, Surya Ganguli, and Jascha Sohl-Dickstein. On the expressive power of deep neural networks. In *Proc. of ICML*, 2017. 4
- [44] Mehdi S. M. Sajjadi, Giambattista Parascandolo, Arash Mehrjou, and Bernhard Schölkopf. Tempered adversarial networks. In *Proc. of ICML*, 2018. 2
- [45] Tim Salimans, Ian J. Goodfellow, Wojciech Zaremba, Vicki Cheung, Alec Radford, and Xi Chen. Improved techniques for training gans. In *Proc. of NeurIPS*, 2016. 2
- [46] Samuel S. Schoenholz, Justin Gilmer, Surya Ganguli, and Jascha Sohl-Dickstein. Deep information propagation. In *Proc. of ICLR*, 2017. 4
- [47] Vaishaal Shankar, Alex Fang, Wenshuo Guo, Sara Fridovich-Keil, Jonathan Ragan-Kelley, Ludwig Schmidt, and Benjamin Recht. Neural kernels without tangents. In *Proc. of ICML*, 2020. 4
- [48] Akash Srivastava, Lazar Valkov, Chris Russell, Michael U. Gutmann, and Charles Sutton. VEEGAN: reducing mode collapse in gans using implicit variational learning. In *Proc. of NeurIPS*, 2017. 2
- [49] Kiran Koshy Thekumparampil, Prateek Jain, Praneeth Netrapalli, and Sewoong Oh. Efficient algorithms for smooth minimax optimization. In *Proc. of NeurIPS*, 2019. 2
- [50] Carl Vondrick, Hamed Pirsiavash, and Antonio Torralba. Generating videos with scene dynamics. In Proc. of NeurIPS, 2016. 1
- [51] Zhou Wang, Alan C Bovik, Hamid R Sheikh, and Eero P Simoncelli. Image quality assessment: from error visibility to structural similarity. *IEEE transactions on image processing*, 2004. 5, 13, 16
- [52] Li Xu, Jimmy S. J. Ren, Ce Liu, and Jiaya Jia. Deep convolutional neural network for image deconvolution. In *Proc. of NeurIPS*, 2014. 1
- [53] Greg Yang. Scaling limits of wide neural networks with weight sharing: Gaussian process behavior, gradient independence, and neural tangent kernel derivation. *CoRR*, abs/1902.04760, 2019. 3, 5

[54] Greg Yang. Tensor programs I: wide feedforward or recurrent neural networks of any architecture are gaussian processes. *CoRR*, abs/1910.12478, 2019. 3

# A. Experiment Settings

This section provides more details about the settings of our experiments.

# A.1. Model Settings

The network architectures of the baseline GANs used in our experiments are based on InfoGAN [7]. We set the latent dimensions, training iterations, and batch size according to the study [31]. The latent dimensions for the generator are all 64. The batch size for all baselines is set to 64. The training iterations are 80K, 100K, and 400K for MNIST, CelebA, and CIFAR-10 datasets, respectively. For the optimizers, we follow the setting from the original paper [23]. Below we list the network architecture of the baselines for each dataset as well as the optimizer settings. Note that we remove all the batchnorm layers for the discriminators in WGAN-GP.

We architect the element network of the discriminator in our GA-NTK following InfoGAN [7] as well, except that the width (or number of filters) of the network is infinite at each layer and no batchnorm layers.

|--|

Discriminator	Generator
Input 28×28×1 Gray image	Input $\in \mathbb{R}^{64} \sim \mathcal{N}(oldsymbol{0}, oldsymbol{I})$
4×4 conv; 64 leaky ReLU; stride 2	Fully Connected 1024 ReLU; batchnorm
4×4 conv; 128 leaky ReLU; stride 2. batchnorm	Fully Connected $7 \times 7 \times 128$ ReLU; batchnorm
Fully Connected 1024 leaky ReLU; batchnorm	4×4 deconv; 64 ReLU. stride 2; batchnorm
Fully Connected 1 output	4×4 decony; 1 sigmoid

Table 3. The architectures of the discriminator and generator in the baseline GANs for the CIFAR-10 dataset.

discriminator	generator
Input 32×32×3 Image	Input $\in \mathbb{R}^{64} \sim \mathcal{N}(oldsymbol{0}, oldsymbol{I})$
4×4 conv; 64 leaky ReLU; stride 2	Fully Connected $2 \times 2 \times 448$ ReLU; batchnorm
4×4 conv; 128 leaky ReLU; stride 2; batchnorm	4×4 deconv; 256 ReLU; stride 2; batchnorm
4×4 conv; 256 leaky ReLU; stride 2; batchnorm	4×4 deconv; 128 ReLU; stride 2
Fully Connected 1 output	4×4 deconv; 64 ReLU; stride 2
	4×4 decony; 3 Tanh; stride 2.

Table 4. The architectures of the discriminator and generator in the baseline GANs for the CelebA dataset.

discriminator	generator		
Input 64×64×3 Image	Input $\in \mathbb{R}^{64} \sim \mathcal{N}(oldsymbol{0}, oldsymbol{I})$		
4×4 conv; 64 leaky ReLU; stride 2	Fully Connected $2 \times 2 \times 448$ ReLU; batchnorm		
4×4 conv; 128 leaky ReLU; stride 2; batchnorm	4×4 deconv; 256 ReLU; stride 2; batchnorm		
4×4 conv; 256 leaky ReLU; stride 2; batchnorm	4×4 decony; 128 ReLU; stride 2		
4×4 conv; 256 leaky ReLU; stride 2; batchnorm	4×4 deconv; 64 ReLU; stride 2		
Fully Connected 1 output	4×4 decony; 32 ReLU; stride 2		
	4×4 decony; 3 Tanh; stride 2.		

Table 5. The optimizer settings for each GAN baseline.  $n_{dis}$  denotes the training steps for discriminators in the alternative training process.

	Optimizer type	Learning Rate	$\beta_1$	$\beta_2$	$n_{dis}$
DCGAN	Adam	0.0002	0.5	0.999	1
LSGAN	Adam	0.0002	0.5	0.999	1
WGAN	RMSProp	0.00005	None	None	5
WGAN-GP	Adam	0.0001	0.5	0.9	5
SN-GAN	Adam	0.0001	0.9	0.999	5

#### A.2. Metrics

The FID scores are computed using the code from the original paper [20]. We sample 2048 images to compute the FID scores. We calculate the AM-SSIM scores using the SSIM settings: Gaussian kernel bandwidth 4, the filter sigma 1.5,  $k_1$  0.01, and  $k_2$  0.03 [51].

## A.3. Hyperparameter Tuning

We tune the hyperparameters of WGAN and WGAN-GP using grid search, whose details are summarized in Algorithm 2.

**Algorithm 2** Grid search algorithm for the hyperparameters of WGAN and WGAN-GP. The algorithm is also used by the second-stage tuning of the hyperparameter  $\lambda$  of GA-NTK, as described in the main paper.

```
Input: Time budget T, starting parameter p

Output: scores

iter \leftarrow 0

scores \leftarrow \phi

while tuning \ time < T \ \mathbf{do}

p_i \leftarrow p \times 2^{iter}

s \leftarrow \text{Run generative algorithms with } p_i

scores \leftarrow scores \cup s

p_j \leftarrow p \div 2^{iter}

s \leftarrow \text{Run generative algorithms with } p_j

scores \leftarrow scores \cup s

p_j \leftarrow p \div 2^{iter}

s \leftarrow \text{Run generative algorithms with } p_j

scores \leftarrow scores \cup s

end

return scores
```

With 3-hour time budget, the hyperparameters we obtained through Algorithm 2 are good enough for reproducing the experiments conducted by the study [32] on mode collapse. In the experiments, the  $\mathcal{P}_{gen}$  of different methods aim to align a 2D 8-modal Gaussian mixtures in the ground truth, as shown in Figure 9.

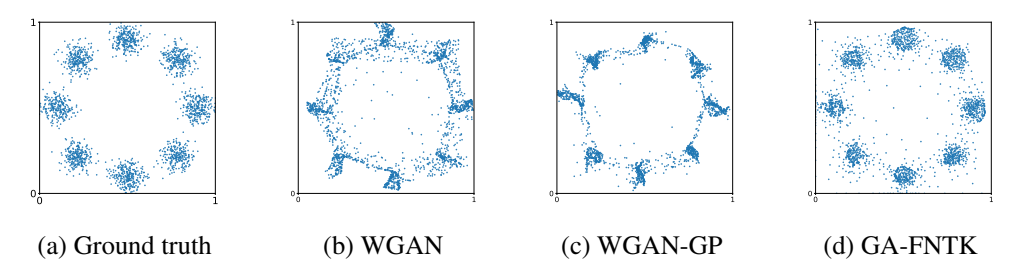


Figure 9. Visualization of distribution alignment and mode collapse on a 2D 8-modal Gaussian mixtures dataset.

# **B.** More Generated Images from GA-NTK

In the following, we show more sample images synthesized by GA-CNTK. All these images are obtained using the settings described in the main paper and the above.

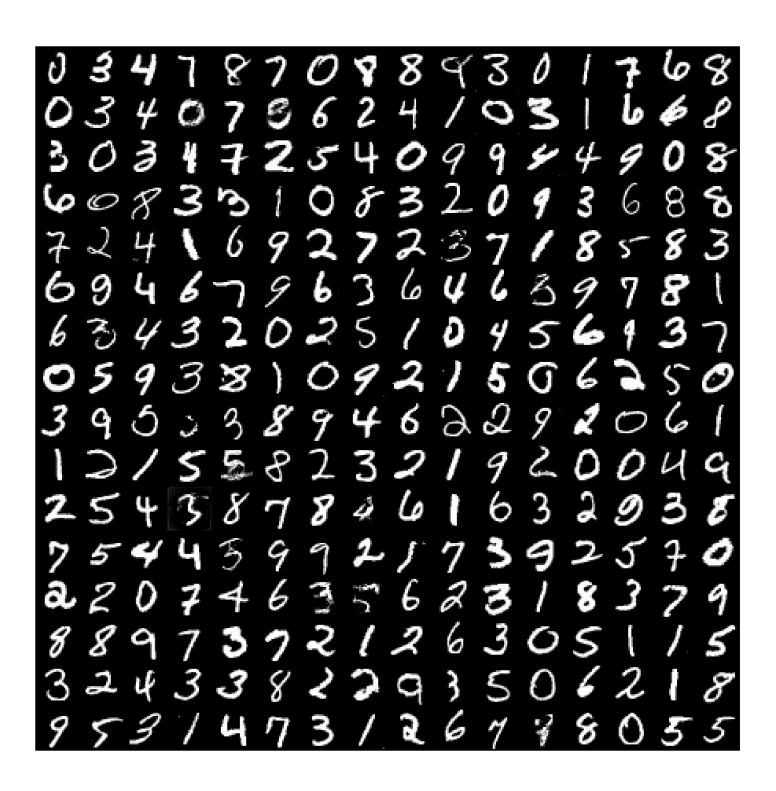


Figure 10. Sample images generated by GA-CNTK on the MNIST dataset.



Figure 11. Sample images generated by GA-CNTK on the CIFAR-10



Figure 12. Sample images generated by GA-CNTK on the CelebA dataset.

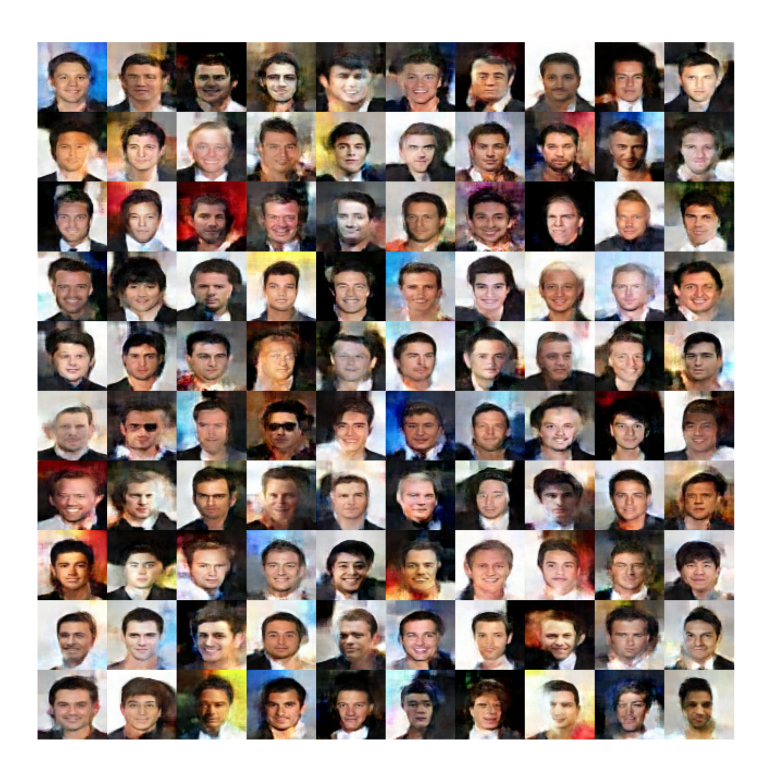


Figure 13. Sample images generated by batch-wise GA-CNTK on the CelebA dataset.

# C. Downgrade Images

As discussed in the main paper, we find that, when the size of training set is small, an image synthesis method may produce downgrade images that look almost identical to some images in the training set. To show this, we show the images from the training set that are the nearest to a generated image. We use the SSIM [51] as the distance measure. Figures 14, 15, and 16 show the results for some randomly sampled synthesized images. As we can see, both GA-CNTK and batch-wise GA-CNTK can generate images that looks less similar to the ground-truth images.



Figure 14. Comparison between the images generated by WGAN-GP and the nearest neighbors (measured by SSIM) from the training set. Images with red bounding boxes are generated images.

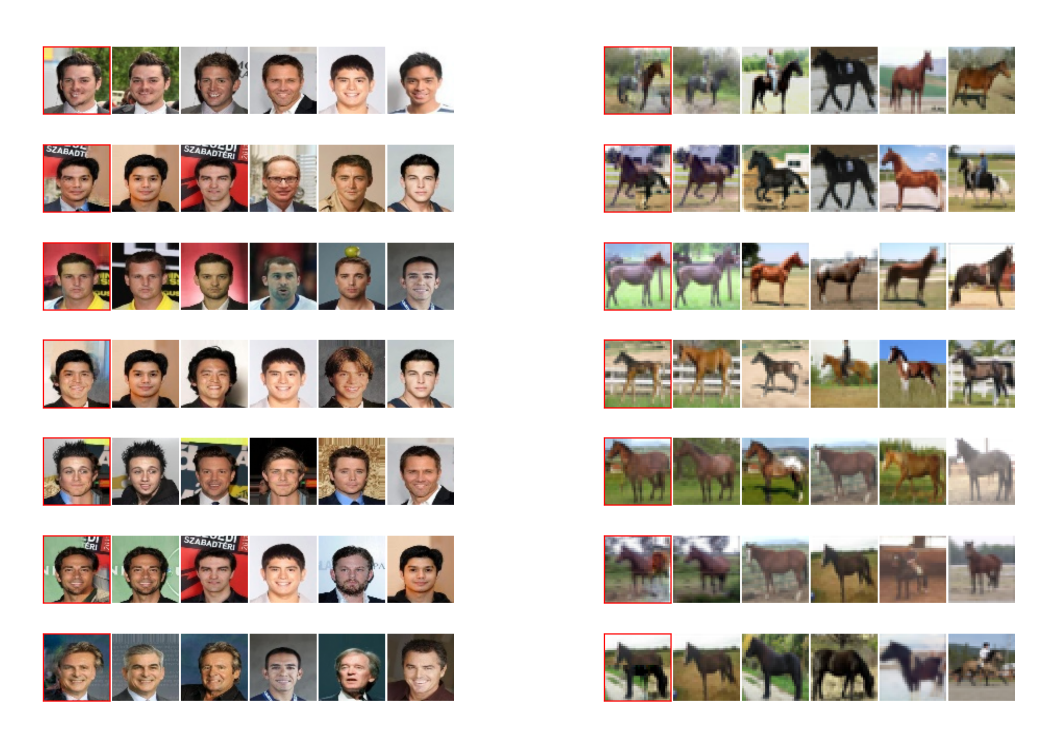


Figure 15. Comparison between the images generated by GA-CNTK and the nearest neighbors (measured by SSIM) from the training set. Images with red bounding boxes are generated images.

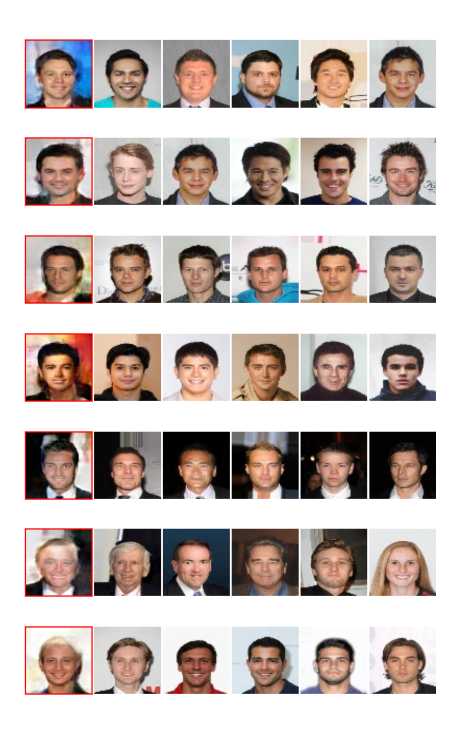


Figure 16. Comparison between the images generated by batch-wise GA-CNTK and the nearest neighbors (measured by SSIM) from the training set. Images with red bounding boxes are generated images.

# D. CelebA-HQ Datasets

Next, we study if GA-NTK can synthesize images with higher resolutions. We train GA-CNTK using the CelebA-HQ dataset [30]. Due to the high memory consumption of GA-CNTK, we resize each image to  $256 \times 256$  pixels and then train GA-CNTK with only 64 images on a single NVIDIA Tesla V100 GPU of 32GB RAM. Figure 17 shows the generated images of  $256 \times 256$  pixels. With only 64 training images, GA-CNTK can generate recognizable faces. However, the patterns in a synthesized image are not globally coherent, as we have discussed in the main paper. This motivates techniques for enhancing the global coherence in GA-CNTK, which we leave as our future work.







Figure 17. Generated data of GA-CNTK on CelebA-HQ dataset